JOURNAL OF GEOPHYSICAL RESEARCH, VOL. 101, NO. C2, PAGES 3545–3560, FEBRUARY 15, 1996

Numerical modeling of suspended sediment due to deep-sea mining

J.A. Jankowski, A. Malcherek and W. Zielke

Institut für Strömungsmechanik und Elektronisches Rechnen im Bauwesen
Universität Hannover, Germany

Abstract. A numerical model was developed in order to estimate the residence time of a sediment plume generated by potential deep-sea mining activities with special attention to discharges in the bottom boundary layer. The site of the Disturbance and Recolonization Experiment (DISCOL) in the Peru Basin in the southeast Pacific Ocean was chosen as a case study. The model includes the actual bathymetry, as well as the characteristic flow patterns of this region. Various aspects affecting the transport and sedimentation of the plume, such as stratification, flocculation in a sediment-laden water column, and the hydrodynamics are discussed in conjunction with field data and studied with the overall aim of providing a reliable risk assessment of deep-sea mining environmental impacts.

Environmental Impact of Sediment Plumes

The future situation in the raw material market raises the question as to the feasibility of the exploitation of mineral deposits located on the seabed, of which manganese nodules are of the greatest interest. The nodules, partially covered by or even buried under thin layers of sediment, form flat horizontal fields on the seafloor at water depths of 4000–5000 m. The deposits and their potential recovery have been intensively researched during the past 20 years [*Bischoff and Piper,* 1979; *Thijsen et al.,* 1981; *Kunzendorf,* 1986, 1988; *Halbach et al.,* 1988; *Padan,* 1990]. Present metal prices and recycling economically limit the feasibility of industrial scale deep-sea mining. This stagnation phase in the deep-sea mining issue allows sufficient time for conducting research on precautionary deep-sea environmental protection and for consultation in the development of technologies with the least possible impact. The subject has gained importance because of the fact that the United Nations International Law of the Sea has been in force since 1994 and will regulate all human activities in international seas, including also environmental issues. Therefore tools are needed which provide a reliable risk assessment of the associated impact, especially because of the uncertainties present in existing estimations.

There are numerous technologies available for marine deposit exploitation. In the case of manganese nodules, the most promising technology is the use of remote-controlled, self-driving collectors working on the ocean floor. These gather the nodules and prepare them for transport to the surface through a riser system [*Amann,* 1989; *Kunzendorf,* 1988]. To minimize mass transport and to avoid the accumulation of superfluous amounts of mining tailings, the sediment needs to be separated from the nodules directly at the source. In this technology the major sediment discharge is into the bottom ocean zone with minor discharge near the surface or at some intermediate depth. The discharged particles will form plumes at different depths that disperse with the currents and, under adverse conditions, may generate turbidity layers [*Ozturgut et al.,* 1981; *Baturin et al.,* 1991].

The plume will consist not only of sediments, but also of small particles broken off from the nodules. Chronic exposure of the organisms to much higher particle concentrations than the ambient $O(10\ \mu g/L)$ and sedimentation levels may occur, since the mining may be nearly continuous. This particulate pollution is expected to influence the marine environment, since, e.g., benthic communities are strongly adapted to very stable conditions. The impact for the biologically productive upper ocean zones may also occur should the mining tailings, from a secondary separation process on board of the mining ship, be discharged at the surface, through a pipeline at some intermediate depth or through an accidental pipeline rupture. However, the major discharge will take place in the bottom ocean zones. Therefore, to evaluate the environmental impact associated with resuspended sediments, an estimation is needed of their residence times and the extent of the area affected by the bottom plumes before they eventually dilute to near-ambient concentrations or deposit at the bottom [*Lavelle et al.,* 1981; *Lavelle and Ozturgut,* 1981; *Lavelle et al.,* 1982; *Thiel,* 1991; *Thiel et al.,* 1991].

Estimations and Previous Models

The main parameter affecting the plume concentration and resedimentation is the in situ sediment settling

Paper number 95JC03564.
0148-0227/96/95JC-03564$05.00

velocity. The situation in the case of deep-sea mining is unusual, because the sediments are resuspended artificially. The particle size distribution, as well as their aggregation order [*Krone,* 1986] directly after discharge, remains unknown, but usually, a total disaggregation of the material is assumed and subsequent flocculation is generally not considered. Therefore simple residence time and the plume extent calculations are based on the assumption of a constant Stokes settling velocity for single particles in a parallel, uniform velocity field. Such straightforward estimations for the very small settling velocities of single clay particles ($O(10^{-6})$ m/s) without consideration of flocculation result in residence times in years and transport distances in hundreds of kilometers.

An analytical model allowing an estimation of the plume transport behavior was developed by *Lavelle et al.* [1981]. In order to obtain a solution for the sediment transport equation, a constant settling velocity in a uniform, horizontal flow field with constant turbulent diffusivities over a flat bottom was assumed. A coefficient controlling the net bottom flux parametrized the sediment deposition. These assumptions allowed a coarse approximation of the plume dispersion [*Malcherek et al.,* 1992].

A calibration of the above analytical model to existing experimental data from plumes induced during mining tests gave mean settling velocities of the order of $10^{-4} - 10^{-3}$ m/s [*Lavelle et al.,* 1981]. These were higher than velocities inferred from laboratory measurements available at that time. This was attributed to higher particle interactions in situ or to the fact that the attenuation signal from the finest particles remained unresolved by the instrumentation [*Lavelle et al.,* 1982; *Ozturgut and Lavelle,* 1986]. Later, an attempt was made to include some further aspects affecting the transport, such as velocity shear, sediment classes characterized by different settling velocities, and scavenging of slower particles by macroparticles (marine snow). The model was two-dimensional with a stationary source and constant current velocities [*Lavelle,* 1987]. The existing models have not included topographic effects, variable currents, and particle interactions.

This underlines the necessity for numerical model development which allows a more advanced approach, involving the three-dimensional and unsteady ambient currents, bottom boundary layer (BBL), realistic bathymetry, stratification, and density flows in the vicinity of the source (a study described by *Jankowski et al.* [1994]), as well as a settling velocity formulation which takes into account flocculation, breakup and scavenging effects. These aspects have not been simultaneously taken into account in previous modeling attempts. Some features of the model, e.g., discharge characteristics, are similar to the previous models, since supporting data are scarce. The developed model also defines the need for experimental data, especially when there are uncertainities in the model parameter values.

Basic Model Assumptions and Features

The numerical model described in this paper has the aim of simulating the dispersion and resedimentation of sediment plumes generated in deep ocean mining areas. The most interesting environmental impact aspects are the plume residence time, the resedimentation rate and intensity, and the unsteady concentration values. The model is designed to simulate the transport processes in the vicinity of the mining area, i.e., at spacial scales where the greatest impact on the marine environment is expected. This type of model can be classified as a mesoscale regional model, where the flow is controlled by large-scale oceanic circulation imposed as boundary conditions at the open boundaries.

The marine systems are characterized by well-defined length and timescale domains associated with the hydrodynamic phenomena (spectral windows [*Nihoul and Djenidi,* 1987]). In this case, the primary effort is to simulate the mesoscale processes (inertial oscillations, tides, diurnal variations superimposed on the relatively stable geostrophic component) at time scales from hours to weeks (frequencies 10^{-5}–10^{-3} rad/s) over distances up to 100 km.

The modeling effort is carried on within the interdisciplinary TUSCH (German Tiefseeumweltschutz, deep sea environmental protection) research group, whose experimental activities (Disturbance and Recolonization Experiment (DISCOL)) are concentrated in the DISCOL Experimental Area (DEA) in the Peru Basin in the

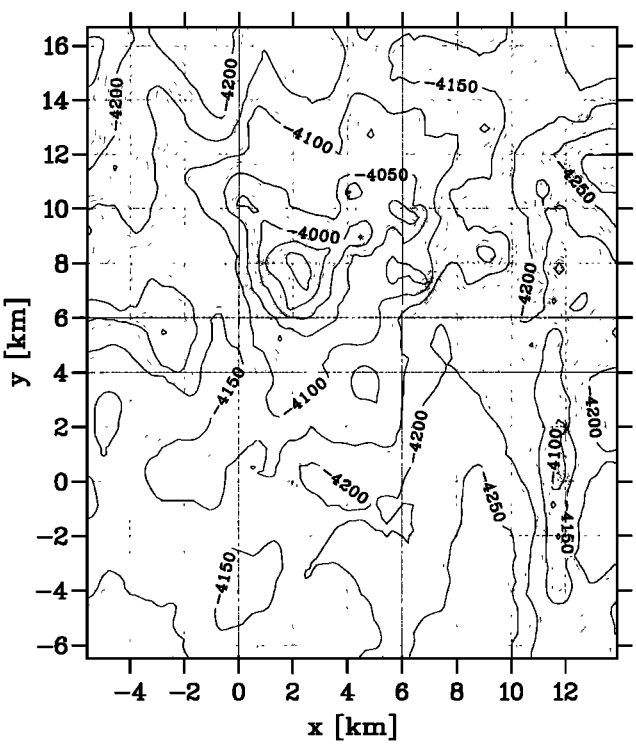

Figure 1. Bathymetry of the modeled area, with the center of the DISCOL Experimental Area (DEA) taken as the coordinate origin (about 7°04′S, 88°28′W).

southeast Pacific Ocean (Figure 1) [*Thiel and Schriever,* 1989, 1990]. Therefore a region of known bathymetry in the vicinity of the DEA (approximately 450 km^2) is treated as a reference area for the model testing and application.

Because the primary aim is to simulate plumes in the bottom boundary layer, including small orographic influences, the model must be both time-dependent and three-dimensional. It is assumed that the current in the homogeneous bottom mixed layer is nearly horizontal [*Armi and Millard,* 1976]. The suspended sediment concentration is treated as the only factor generating stratification and possibly density-driven flows. The time and space resolution must allow a description of the plume near the discharge, starting from the time when the ambient current begins to dominate the plume transport, i.e., after the first phase of dispersion by the eddies in the wake of the machine and the subsequent gravitational collapse in the direct vicinity of the source [*Jankowski et al.,* 1994]. The time and space scales associated with the gravitational plume collapse remain unmeasured, but intensive resedimentation is found up to 100 m or more upstream of the collector tracks. This has been interpreted as the consequence of density flows [*Lavelle et al.,* 1981]. The resulting configuration of the initial plume applied in the model will be discussed further.

The forces generating the current variability are not simulated directly due to the spatial model scale, the features of the deep ocean, and the fact that the boundaries of the computational area are open. The current variability is obtained by calibrating and applying variable pressure fields to the area. This is equivalent to changing the water depth at the boundaries under the assumption that the perturbation pressure is independent of the depth and applying appropriate initial conditions for velocity and surface elevation.

In the subsequent paragraphs the characteristics of the DISCOL area, as well as the mathematical model, are described. Following a discussion of possible settling velocity formulations, the results for a plume discharged by a single collector during 24 hours are discussed. Such emissions appear in mining tests and impact experiments. The model results can also be useful for planning these activities and analyzing the experimental data.

Bathymetry and Hydrography of the DISCOL Experimental Area

A precise description of the hydrography of the region and the hydrodynamic data are provided by *Klein,* [1993]. The measurements relevant to the numerical modeling are described below.

DEA is situated in the Peru Basin (about 7°04′S, 88°28′W) in the vicinity of a potential German mining area. The site is a circle, 3.5 km in diameter, where the bottom was disturbed using a towed plough with the aim of observing subsequent recolonization by local benthic communities [*Thiel and Schriever,* 1989, 1990].

The depth of this site varies between 4140 and 4170 m. The bottom topography was determined from sonar measurements in a rectangular area approximately 20 × 25 km surronding the DISCOL site. About 4 km NW of DEA, an approximately 300-m high protrusion with slopes of maximum 10° is found (Figure 1). The bathymetry of the farther surrounding areas is known with much lower resolution (5′ × 5′).

Long-term current profile measurements were made 15, 30, 50, and 200 m above bottom between September 1989 and January 1992. The time resolution was 1–3 hours. The data analysis published by *Klein* [1993] reveals a current regime characterized by an alternating sequence of relatively strong (> 5 cm/s), quasi-unidirectional currents changing into weak currents (< 1 to 3 cm/s) with great directional variability. The duration of these phases varies between 2 to 5 months without distinguishable periodicity or a seasonal component. The mean scalar velocities are in the range of 2 to 4 cm/s directed west 200 mab and NW 15–50 mab. So-called benthic storms were not observed; current speeds of over 10 cm/s were present for only a few hours. The maximum velocity was 17 cm/s. Figure 2 illustrates the current variability during the first measurement year.

The inertial period $2\pi/f$ for the DISCOL area is about 98 hours, with Coriolis parameter $f = 1.78 \times 10^{-5}$ rad/s. A Fourier analysis, with special attention to the subinertial periods of 3 to 100 hours, reveals the characteristic features of the DISCOL velocities (Figure 3). This shows the following three main components: (1) a slowly varying geostrophic component that may be assumed to be constant for a time period of a week; (2) persistent long waves of periods in the inertial and subinertial range; and (3) tides with mixed, mainly semidiurnal form. The partial tides identified in the energy density spectrum peaks are semidiurnal M_2, S_2, N_2 and diurnal K_1 and O_1.

The conductivity-temperature-depth (CTD) profiles [*Thiel and Schriever,* 1989], up to more than 1000 mab in the deepest zone, show an almost constant temperature (1.8°C) and salinity (34.65 practical salinity units (PSU)). The stratification is stable but very weak. The buoyancy frequency (Brunt-Väisälä frequency)

$$N = \left(-\frac{g}{\varrho} \frac{\partial \varrho}{\partial z} \right)^{1/2} \tag{1}$$

computed using the EOS 80 equation of state for seawater [*UNESCO,* 1987], is 6.41 × 10^{-3} rad/s. Therefore an assumption of neutral stratification is justifiable in modeling the velocity profile in the BBL over a smoothly varying bottom without the presence of suspended matter.

The Taylor analysis for the low-pass filtered data over the entire measurement period, with the minimum wave period of 48 hours, i.e., the tides eliminated [*Klein,*

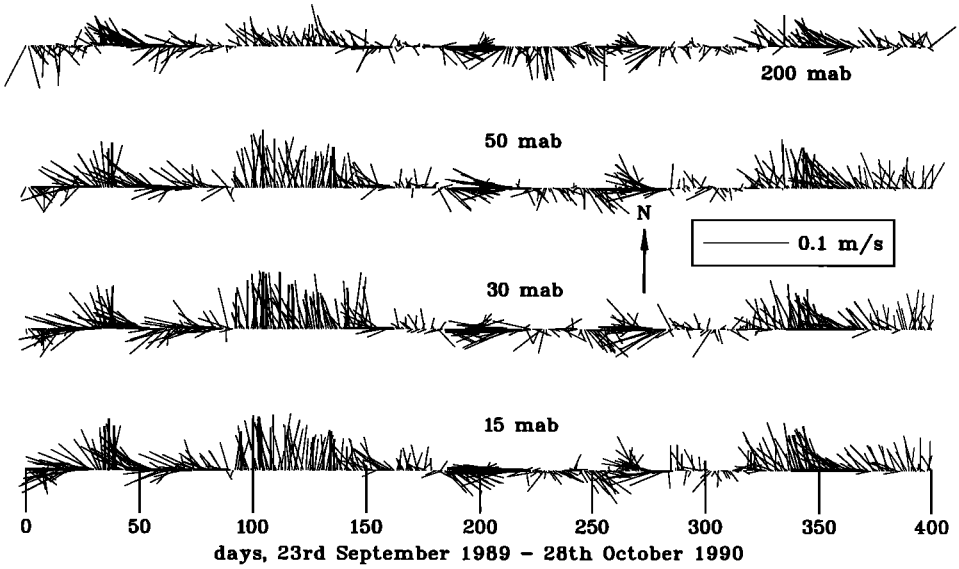

Figure 2. Daily averages of measured velocity vectors in the DISCOL area [after *Klein*, 1993].

1993], yields values in a range of 200 to 700 m^2/s for the horizontal diffusivities, with a higher meridional value. The same procedure for unfiltered data and for time periods of 1 month and for various current regimes yields values of $O(1-10)$ m^2/s.

A good approximation for the reference thickness h_E of a fully developed, steady turbulent BBL in the neutrally stratified case is [*Monin and Ozmidov*, 1985; *Armi and Millard*, 1976; *Bowden*, 1978]

$$h_E = \frac{\kappa u_*}{|f|} \tag{2}$$

where $\kappa = 0.41$ is the von Kármán constant, f is the Coriolis parameter, and u_* is the shear velocity, which is approximated as $u_* = u_g/30$ for the assumed above situation [*Csanady*, 1967]; u_g is the constant geostrophic velocity above the BBL. For DEA (latitude 7°S) and for typical u_g values of 1–15 cm/s one obtains 7–115 m for h_E. The measurements show a high current homogeneity 15-50 mab with small velocity shear. Therefore it can be concluded that these elevations are situated in the upper range of the BBL. Unfortunately, measurements below 15 mab are not available.

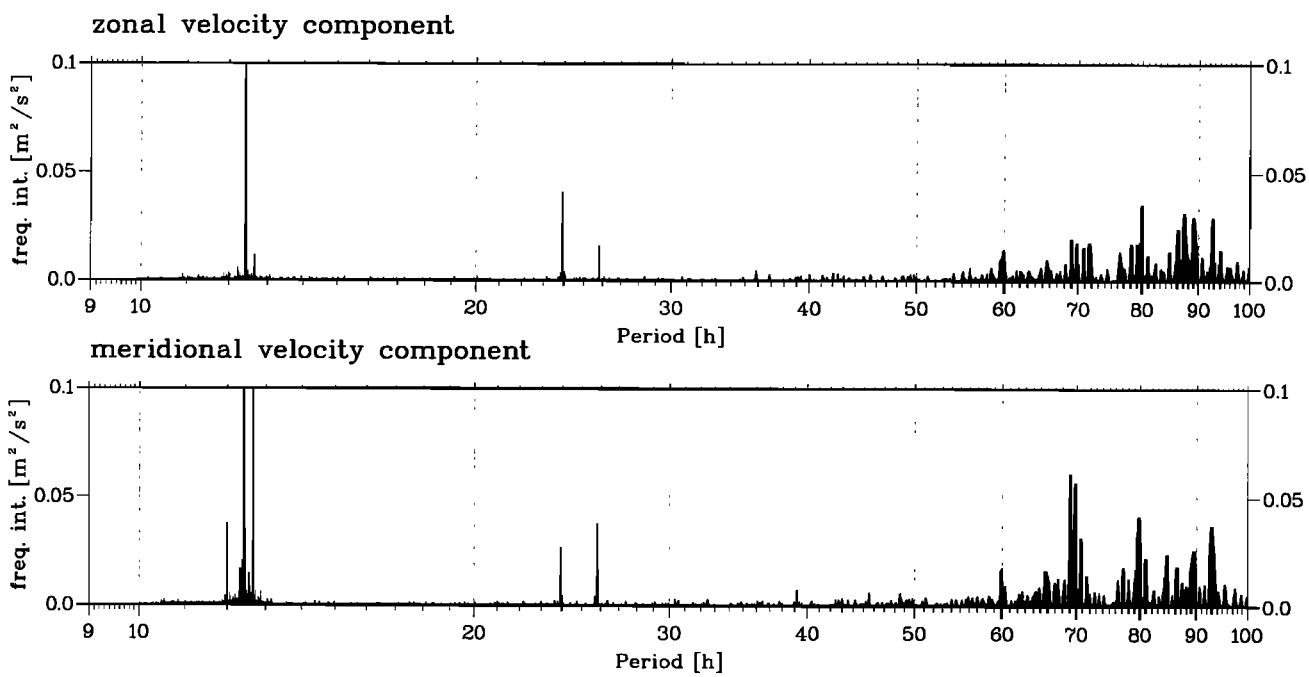

Figure 3. Frequency intensity function (square meters per second squared) of DEA current measurements at the level 30 meters above bottom (mab).

The analyses reveal that the main hydrodynamic features which must be reproduced in the model are (1) currents in geostrophic equilibrium, (2) long gravity waves in the inertial and in the tidal frequency range treated as a perturbation of the geostrophic balance, and (3) the bottom boundary layer. This is in agreement with the model assumptions mentioned in the previous paragraph.

The Three-Dimensional Hydrodynamic Model

The hydrodynamic model is based on the incompressible Navier-Stokes equations with a free surface boundary condition. The numerical code, TELEMAC-3D, was developed by the Electricité de France [*Galland et al.*, 1991; *LeNormant et al.*, 1993]. The momentum and continuity equations obtained using the Boussinesq approximation and neglecting inertial effects in the vertical direction are

$$\frac{\partial u}{\partial t}+u\frac{\partial u}{\partial x}+v\frac{\partial u}{\partial y}+w\frac{\partial u}{\partial z}=-\frac{1}{\varrho_0}\frac{\partial p}{\partial x}+\frac{\partial}{\partial x}\left(\nu_x\frac{\partial u}{\partial x}\right)+\frac{\partial}{\partial y}\left(\nu_y\frac{\partial u}{\partial y}\right)+\frac{\partial}{\partial z}\left(\nu_z\frac{\partial u}{\partial z}\right)+fv \tag{3}$$

$$\frac{\partial v}{\partial t}+u\frac{\partial v}{\partial x}+v\frac{\partial v}{\partial y}+w\frac{\partial v}{\partial z}=-\frac{1}{\varrho_0}\frac{\partial p}{\partial y}+\frac{\partial}{\partial x}\left(\nu_x\frac{\partial v}{\partial x}\right)+\frac{\partial}{\partial y}\left(\nu_y\frac{\partial v}{\partial y}\right)+\frac{\partial}{\partial z}\left(\nu_z\frac{\partial v}{\partial z}\right)-fu \tag{4}$$

$$p=\varrho_0 g\,(S-z)+\varrho_0 g\int_z^S\frac{\Delta\varrho}{\varrho_0}dz \tag{5}$$

$$\frac{\partial u}{\partial x}+\frac{\partial v}{\partial y}+\frac{\partial w}{\partial z}=0 \tag{6}$$

where the Coriolis parameter $f=2\Omega\sin\phi$; $\Omega=2\pi/86164$ rad/s is the Earth's angular rotation velocity; and ϕ is the latitude, negative for the southern hemisphere; ν_i are the eddy viscosity components; $S(x,y)$ is the free surface; ϱ_0 is the water reference density; and $\Delta\varrho=\varrho-\varrho_0$ the density difference. The equations are formulated in the Cartesian coordinate system, where x is directed eastward, y is northward, and z is positive upward. The sediment transport equation, as well as its boundary and initial conditions, are described later.

Model Forcing

In this section the model forcing is described. The main problem is to obtain the mesoscale flow variability in the relatively small domain with open boundaries.

The main energy peaks in the DISCOL velocity data spectrum are associated with waves with a radial frequency greater than the inertial one, $\omega > f$ (Figure 3). This motion can be described using the long gravity waves equations, where the wavelength is much greater than the water depth and rotation plays only a minor role. This type of wave is referred to in the literature as Sverdrup or Poincaré waves and is, for example, responsible for tidal propagation [*LeBlond and Mysak*, 1978; *Platzman*, 1971; *Gill*, 1982; *Pond and Pickard*, 1983].

These waves are treated, for simplicity, as slowly varying, small-amplitude velocity and pressure perturbations around the geostrophic and hydrostatic equilibrium state. Therefore, in the following discussion, the advective accelerations, as well as friction, are neglected.

It should be mentioned that the following mathematical description is valid not only for barotropic waves, but also for baroclinic internal waves in a stratified fluid, because of the existence of separable solutions for velocity components when the horizontal scale of the motion is large when compared with the vertical one. For the barotropic case an appropriate equivalent depth H_e can then be used instead of the full water depth H [*LeBlond and Mysak*, 1978; *Gill*, 1982]. This mathematical equivalency allows a proper description of horizontal velocity components due to waves of different origins using (3)–(6) for the ocean interior directly above the BBL.

Under these assumptions the unforced equations for free long waves in a homogeneous fluid of constant depth (i.e., $H=\text{const}$) are

$$\frac{\partial u}{\partial t}-fv+g\frac{\partial\eta}{\partial x}=0 \tag{7}$$

$$\frac{\partial v}{\partial t}+fu+g\frac{\partial\eta}{\partial y}=0 \tag{8}$$

$$H\left(\frac{\partial u}{\partial x}+\frac{\partial v}{\partial y}\right)+\frac{\partial\eta}{\partial t}=0 \tag{9}$$

Combining (7)–(9), an inhomogeneous wave equation (Klein–Gordon equation) is obtained for the vertical free surface displacement η:

$$\frac{\partial^2\eta}{\partial^2 t}-f^2\eta-gH\nabla_h{}^2\eta=0 \tag{10}$$

The solution has the form of a plane wave

$$\eta=\eta_0\exp[i(k_1x+k_2y-\omega t+\phi)] \tag{11}$$

under the condition that the following dispersion relation is fulfilled

$$\omega^2=gHk_h{}^2+f^2 \tag{12}$$

where $\mathbf{k}_h=(k_1,k_2)$, $k_h=2\pi/\lambda$ is the horizontal wave vector. Assuming the form of (11) for u and v, the velocity components are:

$$u=\frac{\eta_0}{k_h{}^2H}(k_1\omega\cos\psi-k_2f\sin\psi) \tag{13}$$

$$v=\frac{\eta_0}{k_h{}^2H}(k_2\omega\cos\psi+k_1f\sin\psi) \tag{14}$$

with the scalar velocity $|\mathbf{v}|$

$$|\mathbf{v}|=(u^2+v^2)^{1/2}=\frac{\eta_0}{k_hH}(\omega^2\cos^2\psi+f^2\sin^2\psi)^{1/2} \tag{15}$$

where $\psi = k_1 x + k_2 y - \omega t + \phi$ is used for simplicity. The maximum and minimum values are

$$|\mathbf{v}|_{\max} = \eta_0 \omega / k_h H \qquad |\mathbf{v}|_{\min} = \eta_0 f / k_h H \tag{16}$$

As can be seen, the velocity vector draws an ellipse whose major axis is parallel to the propagation direction defined by $\mathbf{k}_h$. The axis ratio of this hodograph is f/ω. For $\omega >> f$ the velocity ellipse is elongated, whereas at near inertial frequencies it is almost circular. The inertial frequency f is the lower frequency limit for long gravity waves. The water particle motion is anticyclonic, i.e., clockwise for $f > 0$ (northern hemisphere) and anticlockwise for $f < 0$ (southern hemisphere).

The maximum velocity values for a given mode (16) are used to obtain proper initial velocity values and the perturbation amplitude η_0 in the model. Approximate values are known from the data analysis. Therefore, for the case of $\phi \neq 0$, we obtain the initial condition for u, v for $t = 0$ and η_0 for $t \geq 0$:

$$\eta_0 = \frac{\omega^2 - f^2}{\omega k_h g} |\mathbf{v}|_{\max} \tag{17}$$

$$u(t=0) = \frac{|\mathbf{v}|_{\max}}{\omega k_h}(k_1 \omega \cos\phi - k_2 f \sin\phi) \tag{18}$$

$$v(t=0) = \frac{|\mathbf{v}|_{\max}}{\omega k_h}(k_2 \omega \cos\phi + k_1 f \sin\phi) \tag{19}$$

The appropriate wavelength can be obtained from the dispersion relation (12).

The waves described by (13) and (14) are superimposed on the geostrophic equilibrium current, which is treated as constant during the simulation (not more than a week). The equilibrium condition is obtained from (7) and (8) by substituting $(u, v) = (u_g, v_g) = \text{const}$:

$$u_g = -\frac{g}{f}\frac{\partial \eta}{\partial y} \qquad v_g = \frac{g}{f}\frac{\partial \eta}{\partial x} \tag{20}$$

In the model the geostrophic component is obtained by applying a constant horizontal pressure gradient at the computational domain boundaries and an appropriate initial velocity condition. In this way the current directly above the BBL can be calibrated using field data [*Jankowski and Zielke*, 1995] (Figure 4).

Description of the Deep-Sea Bottom Boundary Layer

The influence of temperature and salinity stratification in the BBL is assumed to be negligible. In this study the suspended sediment concentration is taken as the only parameter affecting the stratification. The dependence of the fluid density on the dry mass sediment concentration c (in kilograms per cubic meter) is taken as

$$\varrho(p, S, T, c) = \varrho(p, S, T) + \frac{\varrho_{\text{sed}} - \varrho(p, S, T)}{\varrho_{\text{sed}}} c \tag{21}$$

where $\varrho(p, S, T)$ is the water density obtained from the EOS 80 equation of state and ϱ_{sed} is the sediment constituent density. The bottom boundary condition is given by

$$\nu_z \frac{\partial u}{\partial z} = \frac{\tau_b}{\rho} = \frac{u\sqrt{u^2 + v^2}}{C^2} \tag{22}$$

where τ_b is the bed shear stress. The roughness coefficient C is computed by assuming the existence of a

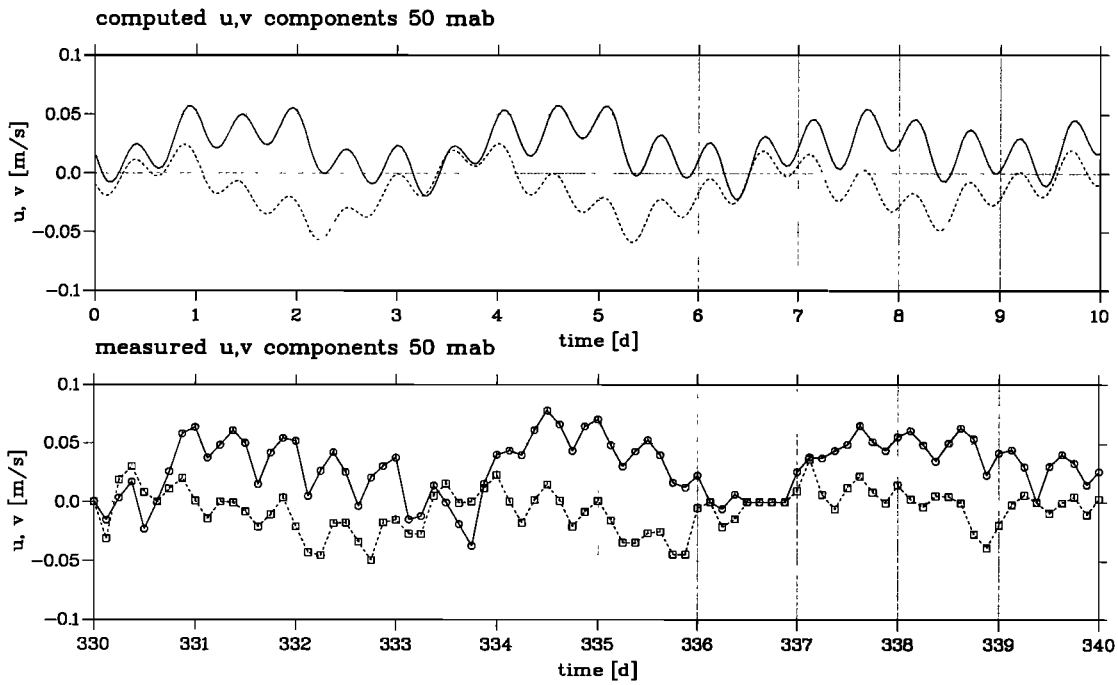

Figure 4. Comparison between the velocity components in the model and in the field at the level 50 mab for days 330–340.

logarithmic velocity profile up to at least one tenth of the distance between the first two planes of the computational mesh in the lowest part of the BBL [*LeNormant et al.*, 1993].

The vertical eddy viscosity and diffusivities are described by a mixing-length model with the damping functions:

$$\nu_z = g(Ri)l^2\sqrt{\left(\frac{\partial u}{\partial z}\right)^2 + \left(\frac{\partial v}{\partial z}\right)^2} \tag{23}$$

$$\nu_{zc} = f(Ri)l^2\sqrt{\left(\frac{\partial u}{\partial z}\right)^2 + \left(\frac{\partial v}{\partial z}\right)^2} \tag{24}$$

using the Richardson number

$$Ri = \frac{-\frac{g}{\rho}\frac{\partial \rho}{\partial z}}{(\frac{\partial u}{\partial z})^2 + (\frac{\partial v}{\partial z})^2} = \frac{N^2}{(\frac{\partial u}{\partial z})^2 + (\frac{\partial v}{\partial z})^2} \tag{25}$$

and the mixing length

$$l = \begin{cases} \kappa z & z_f \le z \le 0.2\delta \\ 0.2\kappa\delta & 0.2\delta < z \le \delta \end{cases} \tag{26}$$

where $\kappa = 0.41$ is the von Kármán constant and z_f is the bottom coordinate. The parameter δ controls the thickness of the BBL [*Mofjeld and Lavelle*, 1984]. The lowest portion of the BBL (approximately between the bottom and 0.2δ) is assumed to consist of a logarithmic layer where the velocity is constant in direction and increases logarithmically in magnitude. In this model the logarithmic layer is situated in the zone where the mixing length increases linearly. In the remaining portion of the BBL (i.e., in the Ekman layer) the mixing length has a constant value given by (26). Following the above mentioned assumptions, both the coefficients δ and C can be calibrated to obtain the velocity profiles in the BBL. As an example, the influence of the parameter δ on the velocity and eddy viscosity profiles for a 5 cm/s geostrophic equilibrium current is illustrated in Figure 5.

Vertical mixing is damped when stratification is present. This effect is taken into account in (23) and (24) by using the damping functions $g(Ri)$ and $f(Ri)$, derived from a second-order turbulence model [*Sheng*, 1983].

The Sediment Transport Model

The sediment transport equation is given as

$$\frac{\partial c}{\partial t} + u\frac{\partial c}{\partial x} + v\frac{\partial c}{\partial y} + w\frac{\partial c}{\partial z} + \frac{\partial (w_s c)}{\partial z} = \frac{\partial}{\partial x}\left(\nu_{xc}\frac{\partial c}{\partial x}\right) + \frac{\partial}{\partial y}\left(\nu_{yc}\frac{\partial c}{\partial y}\right) + \frac{\partial}{\partial z}\left(\nu_{zc}\frac{\partial c}{\partial z}\right) + q_c \tag{27}$$

where c is the dry mass sediment concentration, w_s is the settling velocity, ν_{ic} is the eddy diffusivity, and q_c is the source term. The value of the settling velocity in the assumed coordinate system is negative. In the following text, absolute values are used for simplicity.

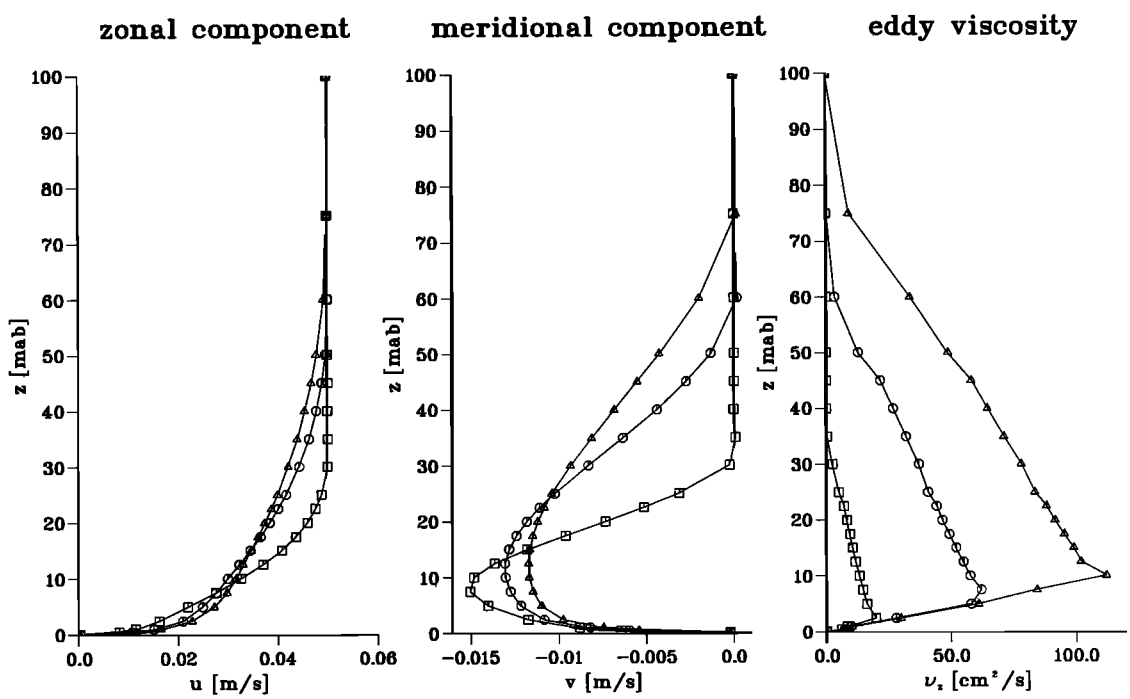

Figure 5. Influence of the coefficient δ controlling the mixing-length distribution on the velocity and vertical eddy diffusivity profiles for a constant geostrophic velocity component of 5 cm/s above the bottom boundary layer (BBL). A constant value of $C = 2$ (giving almost maximum bottom shear) is assumed; squares denote $\delta = 10$ m; circles $\delta = 30$ m; and triangles $\delta = 50$ m.

The reported maximum sediment concentrations, in the range of 10 g/L [*Lavelle et al.*, 1981], are such that the volume fraction occupied by the sediment can be neglected in the continuity equation (6).

The net sediment flux at the surface is zero:

$$\left[w_s c - \nu_{zc}\frac{\partial c}{\partial z}\right]_{\text{surf}} = 0 \tag{28}$$

Erosion and sedimentation at the sediment-water interface are functions of the bed shear stress τ_b, (22), the critical shear stress of deposition τ_{cd}, and the critical shear stress of erosion τ_{ce}. If the bed shear stress exceeds the critical deposition shear stress, a particle settled on the bed is immediately resuspended. If the bed shear stress is less than τ_{ce}, no erosion occurs. Consequently, the bottom boundary condition is formulated as follows

$$\left[w_s \cdot c - \nu_{zc}\frac{\partial c}{\partial z}\right]_{\text{bot}} = w_s c|_{\text{bot}} f_d + M_{\text{res}} f_e \tag{29}$$

where the probabilities for deposition and erosion are given by [*Krone*, 1962]

$$f_d = \begin{cases} 0 & \tau_b \geq \tau_{cd} \\ (1 - \tau_b/\tau_{cd}) & \tau_b < \tau_{cd}, \end{cases} \tag{30}$$

$$f_e = \begin{cases} 0 & \tau_b < \tau_{ce} \\ (\tau_b/\tau_{ce} - 1) & \tau_b \geq \tau_{ce}. \end{cases} \tag{31}$$

The resuspension rate M_{res} and the critical stresses τ_{ce} and τ_{de} must be obtained from empirical formulations. When sediment is discharged in larger concentrations into a deep-sea boundary layer, the reduced vertical mixing due to the stable stratification has an important influence on the concentration distribution in the first stages of plume transport [*Jankowski et al.*, 1994].

Settling Velocity, Flocculation and Scavenging Effects

The data depicting the particle size distribution from the upper centimeter of the DEA bottom sediments show that the particle diameter percentage frequency distribution for $d < 60$ μm equals approximately 83% [*Klein*, 1993]. No site-specific measurements for the settling velocity or information about the density and aggregation order of these sediments, when brought into suspension, are available. Therefore the sediment plume introduced by a nodule collector is assumed to have a particle distribution similar to that of the bottom sediment. The Stokes' settling velocities given in Table 1 are computed according to the method described by [*McCave*, 1984], taking into account the fact that the particles are aggregates and consist of mineral and organic matter. The particle bulk density is assumed to be a function of the particle diameter d. For the computation of w_s the Stokes formula is used, $w_s = \Delta\varrho g d^2/18\mu$, where $\Delta\varrho$ is the density between the in situ aggregate bulk density and the surrounding fluid, $\mu = 1.7 \times 10^{-3}$ kg/ms, the in situ dynamic viscosity of seawater. From the given percentage diameter distribution $n(d)$ from DEA, the mean settling velocity w_{sm} of the composite sediment spectrum can be calculated from

$$w_{sm} = \frac{\sum_i w_{si} c_i}{\sum_i c_i} \tag{32}$$

where c_i are the dry mass concentrations of the fraction characterized by the diameter d_i. Taking the values d_i in the middle of the intervals defined in Table 1 (3 μm for the finest and 100 μm for the largest particles), the lowest value for $w_{sm} \approx 2.2 \times 10^{-4}$ m/s.

Particles defined through $d < 63$ μm have the characteristic that the interparticle forces may be of the order of the inertia and drag forces acting upon them. Owing to cohesive forces, these particles can form large flocs containing a large number of single grains (flocculation). Such flocs, when compared with the original particles, have different densities, sizes, and shapes. Their settling behavior differs greatly from that of single particles. In regions of greater turbulence, large flocs can be broken down into smaller ones (breakup).

Two mechanisms have to be considered in order to assess the influence of flocculation on the settling behavior of a sediment plume: collision which bring particles together and processes which form aggregates following a collision. The collision mechanisms are (1) Brownian motion, (2) turbulent velocity fluctuations, and (3) differential settling. Differential settling is related to larger particles which overrun the finer, slower settling ones, collect them, and build larger aggregates which move more rapidly downward. Relations for the collision probabilities β_{ij}, defined as the probability that two particles of the diameters d_i and d_j trapped in a unit volume collide in a unit of time (Figure 6), can be derived from flocculation theory [*Friedlander*, 1977; *McCave*, 1984].

Figure 6 shows that only Brownian motion has a significant influence on the flocculation behavior of the smallest particles, assuming that each collision forms an aggregate. On the other hand, the flocculation of

Table 1. Settling Velocities of DISCOL Experimental Area Sediments

d, μm	$\Delta\varrho$, kg/m^3	w_s, m/s	$n(d)$, %	
500	9.6	8.70×10^{-4}		
200	31.5	4.58×10^{-4}	> 100 μm:	14
100	77.6	2.82×10^{-4}		
60	149.0	1.95×10^{-4}	$60 - 100$ μm:	3
40	211.1	1.22×10^{-4}	$40 - 60$ μm:	7
20	282.0	4.10×10^{-5}	$20 - 40$ μm:	36
10	378.0	1.37×10^{-5}	< 20 μm:	40
5	506.0	4.60×10^{-6}		

Values were computed according to *McCave* [1984]. Variables are d, particle diameter, $\Delta\varrho$, density difference, w_s, sediment settling velocity, and $n(d)$, percentage diameter distribution.

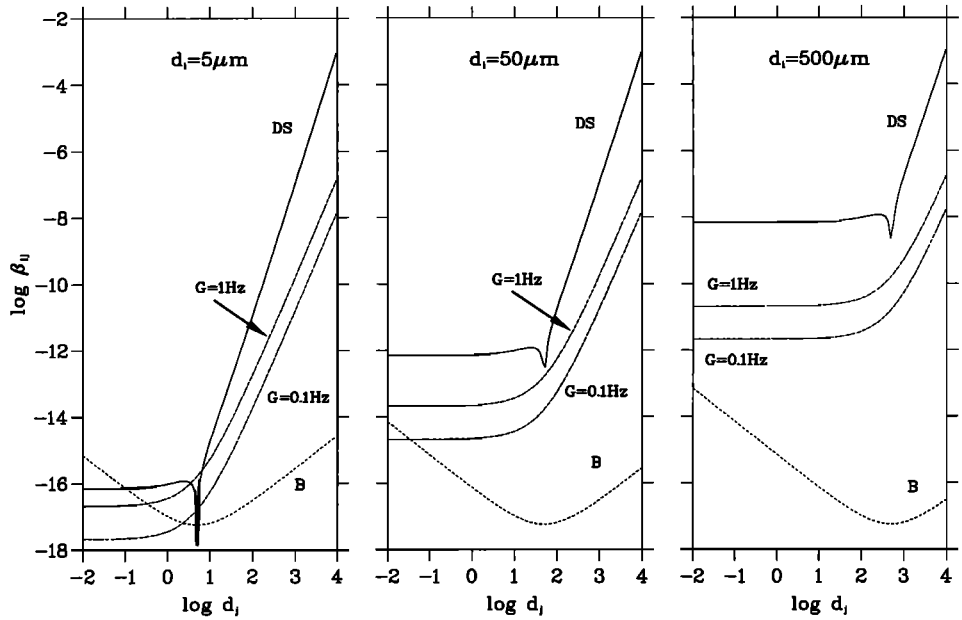

Figure 6. Comparison of the collision coefficients β_{ij} (cubic meters per second) of particles with d_i =5, 50, 500 μm due to Brownian molecular motion (B), turbulent shear (G), and differential settling (DS) as the function of particle diameters d_j (micrometers) plotted for deep-sea conditions.

larger particles is influenced mainly by differential settling and high turbulence intensities.

The parameter which controls breakup and flocculation due to the velocity shear is the absolute velocity gradient G defined as

$$G = \left(\frac{\varepsilon}{\nu}\right)^{1/2} \tag{33}$$

where ε is the turbulent energy dissipation and ν is the molecular viscosity. The value of ε for the deep-sea BBL is of the order of 10^{-8} m^2/s^3 [*Monin and Ozmidov*, 1985]. G can be regarded as the velocity gradient at the spatial scale of the clay flocs.

The absolute velocity gradient plays an important role in the assessment of breakup effects due to turbulent shear. It can be shown by dimensional analysis that the size of the microscale eddies determining the absolute velocity gradient (the Kolmogorov length) is given as

$$\lambda = \left(\frac{\nu^3}{\varepsilon}\right)^{1/4} \tag{34}$$

When an aggregate is smaller than λ, the inertial force resulting from its movement in a microscale eddy is responsible for its possible breakup. Shear force will act on the floc when the floc is larger than the eddy. It can be shown that the shear force is much larger than the inertial force. Thus one can assume that the aggregate will break up when it is larger than the Kolmogorov length.

For $G \approx 0.1$ Hz, typical for conditions in the deep-sea BBL, the Kolmogorov length is about 5 mm. It can be concluded that flocs smaller than this size will settle without being broken up into smaller ones. This means that the settling of the discharged deep-sea sediment plume far enough from the mining vehicle will take place without breakup processes.

The characteristic flocculation time is defined as the time necessary for the original number of particles of one diameter class to diminish tenfold due to one of the above mentioned flocculation mechanisms. Figure 7 presents the characteristic flocculation times associ-

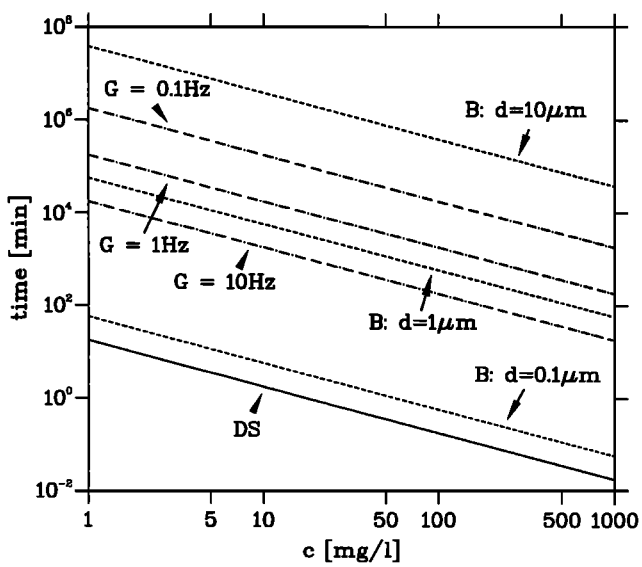

Figure 7. Characteristic flocculation times associated with Brownian motion (B), turbulent shear (G), and differential settling (DS) as functions of the suspended sediment concentration for deep-sea conditions.

ated with the three different flocculation mechanisms [*Malcherek,* 1995] under deep-sea conditions (temperature 1.8°C, water depth of about 4200 m, dynamic viscosity $\mu = 1.7 \times 10^{-3}$ kg/ms, particle density distribution according to *McCave* [1984]).

The analysis shows that differential settling dominates the other mechanisms, especially for the most important case of low concentrations in diluted plumes away from the discharge source. Brownian motion and turbulent shear can remarkably contribute to a reduction of the plume concentration when the concentrations are high or when high turbulence is expected, i.e., in the immediate vicinity of the collector (concentrations up to 10 g/L or higher [*Lavelle et al.,* 1981]).

Analyzing the differential settling processes, there are two possible origins of the larger particles which scavenge smaller ones as follows: (1) external particles originating in the upper ocean layers (marine snow) and (2) aggregates occurring in the discharged plume. The influence of the former particles is of importance only in the areas of a large biological productivity and only when they are not dissolved or destroyed before reaching the BBL.

In some areas the vertical mass flux is dominated by rapid settling of large, amorphous aggregates of diverse, mostly biological origin, so-called marine snow (diameter $O(0.1 - 1$ mm), settling velocities up to 1 mm/s). These sweep large ranges of the water column, collecting and transporting finer particles downward. When the difference between diameters of the interacting particles is large, differential settling dominates thoroughly the process of mass removal from the plume, which can be modeled using an additional sink term in the transport equation (27).

The total water column volume swept by n marine snow particles in the time increment dt is $n\pi D^2 w_s dt/4$, where w_s is the settling velocity and D is the impact diameter approximately equal to the particle diameter. If the fine particles in the plume, which are scavenged with the efficiency β ($0 \leq \beta \leq 1$), have the mass concentration c, the loss of plume mass dc per unit volume in the time increment dt can be written as

$$dc = -\frac{\pi}{4}\beta n D^2 w_s c dt \tag{35}$$

which leads to the definition of the scavenging rate α

$$\frac{dc}{dt} = -\alpha c = -T_\alpha^{-1} c \tag{36}$$

as the inverse of the characteristic scavenging timescale T_α. If scavenging is the only process affecting particle removal from the water column, the concentration c would be reduced by the factor of e^{-1} in the time T_α.

According to the data from the Panama Basin at a depth of 3800 m [*Asper,* 1987], the scavenging timescales for particle number concentrations $O(10^3$ m$^{-3})$, diameters of 2–4.6 mm, and settling velocities of $O(4 \times 10^{-4}$ m/s) are in the range of one week. The concentrations in low-productivity areas may be $O(20 - 60$ m$^{-3})$ [*McCave,* 1984]. As such, T_α will be in the range of 100 to 300 days, making this effect insignificant in the model timescales. In DEA, marine snow has not been quantified.

The second and most important source of the larger particles is the plume itself. In this case the influence of the flocculation may be modeled using one of the most common settling velocity formulas for cohesive sediment transport. This is based on the assumption that the flocculation and therefore also the mean settling velocity are proportional to the suspended sediment concentration

$$w_s = kc^m \tag{37}$$

where k and m are empirical constants [e.g., *Dyer,* 1989; *van Leussen,* 1988, 1994]. Unfortunately, data about the in situ cohesive properties of the deep-sea sediments are too scarce to allow a calibration of (37) in a nonspeculative way, especially in the case of the deep-sea mining discharges [*McCave and Gross,* 1991]. Laboratory experiments using sediments from the equatorial Pacific mining areas have shown that flocculation effects are significant at concentrations above 100 mg/L [*Ozturgut and Lavelle,* 1986].

In the simulations described in this paper a constant mean sediment settling velocity is assumed. An empirical flocculation model is possible when the aggregate size distribution in the discharged plume and the settling velocity as a function of the concentration and the turbulence characteristics in the BBL are known.

The possibility of using a spectrum of noninteracting sediment classes characterized by different settling velocities was rejected, because the dependence of the plume concentration on the settling velocity spectrum is insignificant when compared with the uncertainties associated with other parameters [*Lavelle,* 1987]. An attempt to describe flocculation effects by assuming an interaction between classes was also rejected due to the uncertainity in the interaction rates. A parameter study with a broad range of constant mean settling velocities was performed in order to estimate the uncertainities.

The situation described above is no longer valid in the direct vicinity of the collector. Owing to the vehicle movement and the jet-like sediment discharge behind it, high turbulence intensities, as well as density effects, occur. These have to be taken into account in a numerical model, e.g., through a higher-order closure scheme. The effects of breakup in zones of higher turbulence, as well as subsequent flocculation in an intermediate turbulence zone, also have to be considered. This is generally possible using the settling velocity concept proposed by *Dyer* [1989] and successfully applied to the turbidity zone in an estuary [*Malcherek et al.,* 1996]. The experimental work planned for 1996 by the TUSCH Group should provide more information on the cohesive properties of the sediments discharged during deep-sea mining operations.

Modeling the Sediment Source

The initial sediment concentration, discharge rate, and the particle characteristics depend strongly on the

technology used and the properties of the bottom sediments. These parameters remain mostly unmeasured or, at best, only approximately known. Data were collected during mining tests about 15 years ago [*Lavelle et al.*, 1981; *Lavelle*, 1987] and during experiments with a disturber simulating the collector emission [*Trueblood*, 1993]. Assumptions are inevitable, and further field data are urgently needed.

In previous models describing plume dispersion, the discharge has been modeled as a stationary linear source whose intensity increases exponentially toward the ocean bed [*Lavelle et al.*, 1981; *Lavelle*, 1987; *Malcherek et al.*, 1992]. This is believed to be a good representation of the concentration distribution near the collector, after the initial settling of the dense plume and after the density-driven momentum has been dissipated by frictional effects. The evidence of the density flows has been observed in the vicinity of collector tracks. The density of the sediment-laden water was estimated to be up to 3% above ambient [*Lavelle et al.*, 1981]. Density flows are even believed to be the most important effect controlling the transport of the dense plume resulting from tailing discharge in the bottom zones [*Baturin et al.*, 1991].

The simulation of a stationary source [*Jankowski et al.*, 1994] showed that an exponentially distributed mass emission $O(10$ kg/s) in the BBL leads to a flat, near-bottom plume due to density flows, stratification, and shear diffusion. It may also extend against the ambient current as a result of initial density flows. The near-field effects which control the initial spreading play an important role in the subsequent plume transport to be described by the mesoscale model addressed in this paper.

The collectors do not form a stationary source as they move on the bottom, covering distances of a few kilometers or even greater relative to the position of the mining ship. Their velocities, of up to 1 m/s, are much higher than the ambient current. A single collector moving in alternate directions, usually on a linear path, can be represented as a mass source moving in an oscillatory way. In the sediment transport equation (27) the emission is represented by the source term $q_c(x, y, z, t)$. At each time step the position of the source changes. In this application the collector was assumed to move with a velocity of 0.4 m/s (1440 m/h) on a linear path oriented SW-NE centered in the DISCOL site, altering its direction each hour.

The discharge of a modern collector is 1–50 kg/s, depending on the technology and the amount of mass in the upper layer of bottom sediments available for resuspension [*Ozturgut et al.*, 1981]. The mining simulators used in impact experiments produce similar emissions, approximately 5 kg/s [*Brockett and Richards*, 1994]. The discharge here is assumed to be constant along the path and equal to 10 kg/s dry weight of sediment. The collector works continuously for 24 hours, discharging a total of 864 tons of sediment.

The results of *Jankowski* [1994] are taken into account in the source formulation. The initial horizontal concentration distribution is assumed to be Gaussian, with a radius approximately equal to the standard deviation $\sigma = 100$ m. This defines the spatial resolution in the vicinity of the moving source. An exponential vertical distribution in the form $\exp(-\gamma z)$ is assumed, with $\gamma = 0.5$ m^{-1}. The emission reaches zero 15 m above the bottom.

Results for DISCOL Experimental Area

The computational mesh represents a rectangular area about 19 km wide (W–E) and 23 km long (N–S) with a seabed elevation –4320 to –3880 m. It consists of 2298 nodes forming 4502 triangular elements with 23 vertical planes, i.e., a total of almost 10^5 prismatic three-dimensional elements. These planes are logarithmically distributed near the bed and uniformly between 100 m and 500 mab. The highest mesh level represents the model surface. This vertical distribution allows a proper description of the influence of the bottom topography on the velocity field and the spreading of a near-bottom plume. The horizontal resolution varies within 500–700 m, except in the direct vicinity of DEA (a rectangle 1853 × 1853 m). Here a finer resolution of approximately 100 m allows proper numerical description of the moving sediment source.

To provide a realistic assessment of the plume residence time, the parameters whose values are approximately known were varied within ranges considered realistic. The residence time is defined here as the time in which the suspended mass is diminished e-fold, (i.e., the time after which 63% of sediment deposits). The sensitivity analysis is described as follows.

1. The following two different characteristic flow scenarios above the BBL (Figure 8), representative for this region are used: first, relatively intensive NW directed current modified by tides as well as 3-day period subinertial waves, and second, only tidal-induced currents. The model describes the current variability in the ranges between tidal and geostrophic velocity components for up to 1 week. The higher-frequency variability must be modeled by choosing an appropriate eddy diffusivity value. In this case a horizontal diffusivity for sediment of 1.0 m^2/s was used. A value of 0.1 m^2/s was also tested for comparison (Figure 9c).

2. The mean settling velocity w_s is assumed to be constant. The reference value $w_s = 10^{-4}$ m/s is assumed. This is approximately 50% of the settling velocity resulting from the estimations using the particle size distribution according to *McCave* [1984]. Because of the uncertainities associated with the site-specific diameter distribution [e.g. *McCave and Gross*, 1991], constituent density, and the aggregation order, values of 5.0×10^{-4} m/s and 5.0×10^{-5} m/s were used for comparison (Figure 9a). For $w_s = 10^{-5}$ m/s (finer particle fraction) the scavenging effect with a timescale T_α of 1 week was studied (Figure 9e). It is assumed that no erosion of the deep-sea bed occurs in the low energetic BBL and that the probability of deposition is 1; that is, each sediment particle reaching the bottom will be deposited.

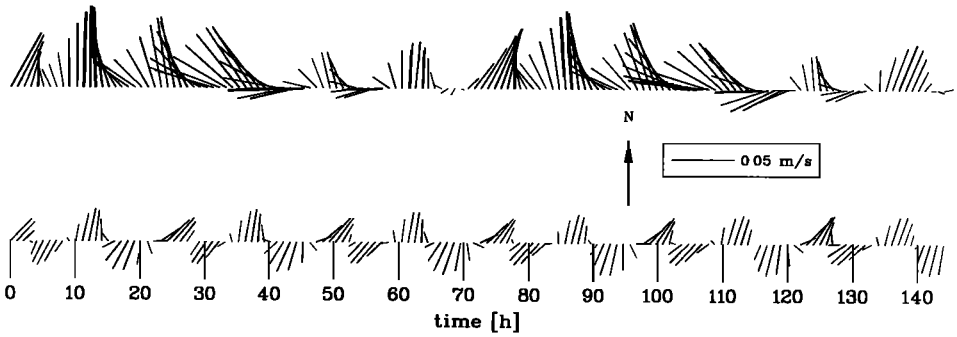

Figure 8. Two flow scenarios used in the parameter study. Plots of velocity each hour for are flows at the level of 100 m above bottom.

3. Three different values of the parameter δ (10, 30, and 50 m), controlling the BBL thickness, the vertical velocity profile, and the value and distribution of the vertical diffusivity were tested. The bottom roughness parameter C was set to 2 (Figure 9b; compare Figure 5).

4. A sensitivity study on the influence of sediment-induced density differences on the plume spreading and deposition characteristics was carried out by using, on the one hand, $\varrho_{\text{sed}} = 2650$ kg/m^3 in the equation of state (21) and, on the other hand, neglecting the sediment influence term in this equation completely [$\varrho_{\text{sed}} = \varrho(p, s, T)$].

The results for sediment deposition for various parameter combinations are shown in Figure 9. Unless stated otherwise, the flow scenario 1 and $\nu_{xc} = \nu_{yc} = 1.0$ m^2/s, $\delta = 10$ m, $C = 2$, and $w_s = 10^{-4}$ m/s are taken as reference values.

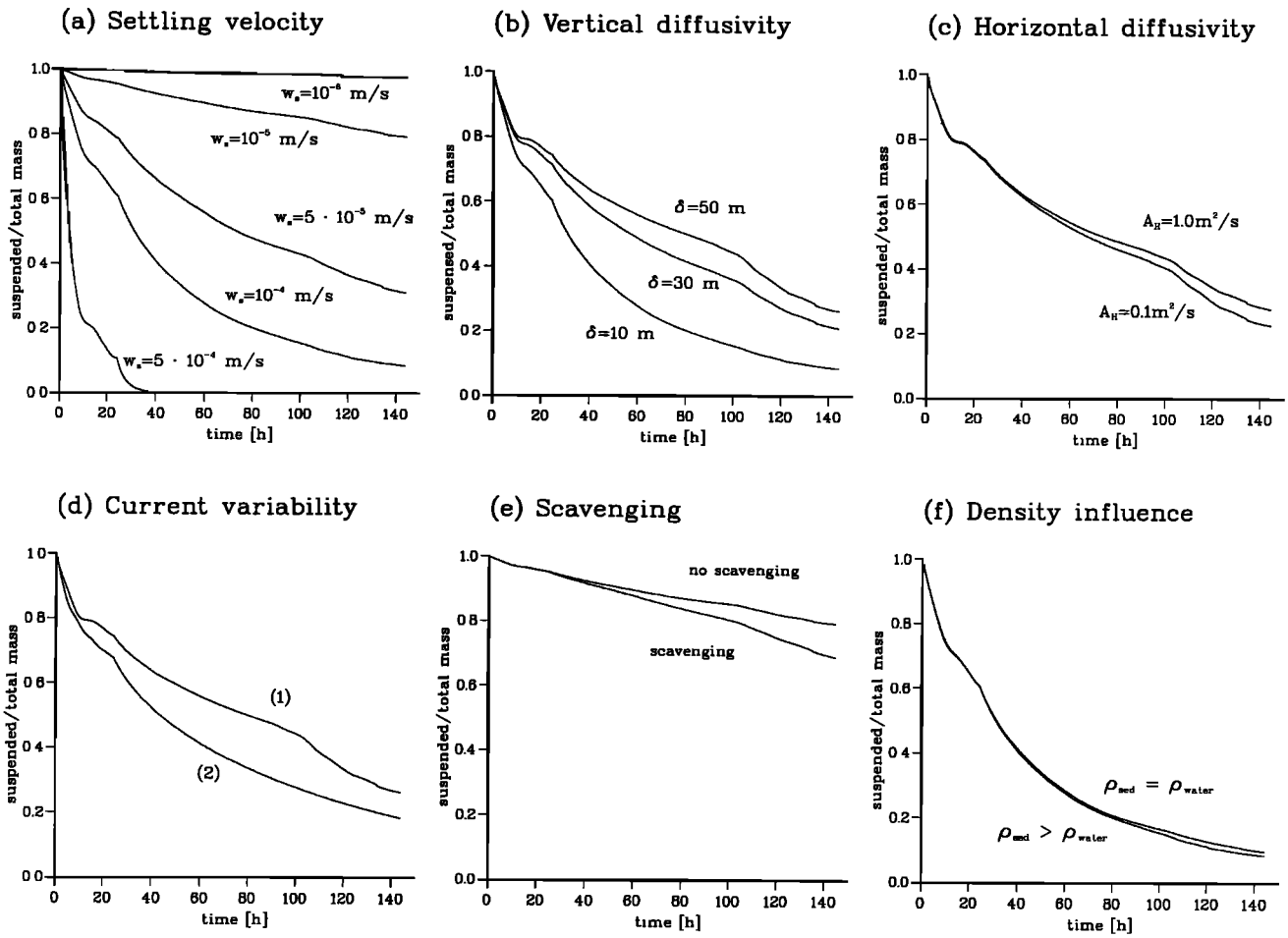

Figure 9. Sensitivity analysis on the sediment deposition from the water column for (a) settling velocity, (b) vertical diffusivity, (c) horizontal diffusivity, (d) current variability, (e) scavenging, and (f) density influence.

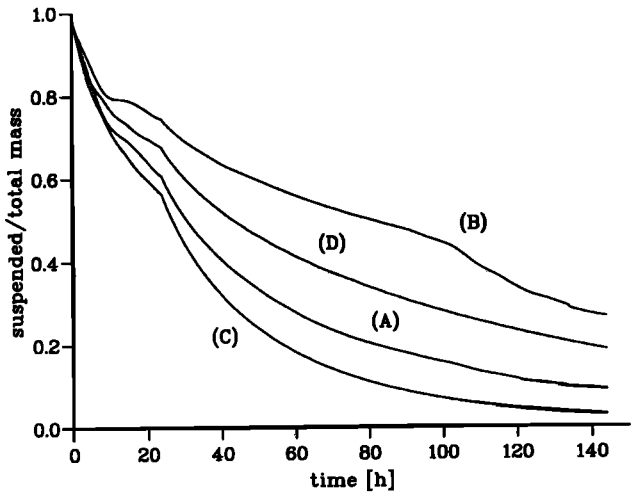

Figure 10. Estimation of the plume residence time.

Table 2. Maximum Concentrations and Deposition

Current, Curve	δ, m	T_r, hours	C_r, mg/L	D_r, g/m^2	C_{max}, mg/L	D_{max}, g/m^2
1, A	10	44	3.4	545	0.08	546
1, B	50	114	0.17	347	0.12	348
2, C	10	36	30.0	670	0.13	770
2, D	50	72	2.4	607	0.47	637

Maximum concentrations and deposition C_r and D_r are after the residence time T_r. C_{max}, D_{max} are after 6 days. For different current scenarios and values of parameter δ. Mean settling velocity is $w_s = 10^{-4}$ m/s, horizontal diffusivity is $\nu_{xc} = \nu_{yc} = 1.0$ m^2/s. See Figure 10.

The following conclusions can be drawn from the sensitivity analysis (Figures 9a-9f). (a) The mean settling velocity has the most important influence on the sediment deposition. For comparison, results for $w_s = 10^{-5}$ m/s and $w_s = 10^{-6}$ m/s are shown. Figure 9a also shows the strong influence of the residence time on the value of w_s. It ranges for the assumed settling velocities between 6 hours and 5 days. The associated concentrations after 3 and 6 days are given in Table 3. (b) The choice of the BBL thickness and the value and distribution of the vertical diffusivity are important parameters which influence the residence time. (c) An oscillatory, tidal current, which lacks a strong advective component, locally accelerates the deposition around the emission area (for $\delta = 50$ m). (d) A lower horizontal diffusivity allows the formation of a denser plume with slightly higher deposition (for $\delta = 50$ m). (e) The possible scavenging by marine snow may be an important process in the removal of the finest particles from the water column in the areas where this phenomenon occurs (here $w_s = 10^{-5}$ m/s). (f) The influence of sediment-induced density differences reduces slightly the plume residence time.

Furthermore, an estimation of the residence time is shown in Figure 10. In this case ($w_s = 1.0 \times 10^{-4}$ m/s), different current scenarios and δ values are taken. A residence time of 2–5 days for the strong flow scenario 1 (curves A and B) and 1.5–3 days for the weak flow (scenario 2, curves C and D) is obtained (see also Table 2).

As an example, the horizontal plume, approximately 1 mab, and vertical sections, south-north, through the point (0, 0) after 3 days, as well as the redeposition patterns in the vicinity of the test area, are given in Fig-

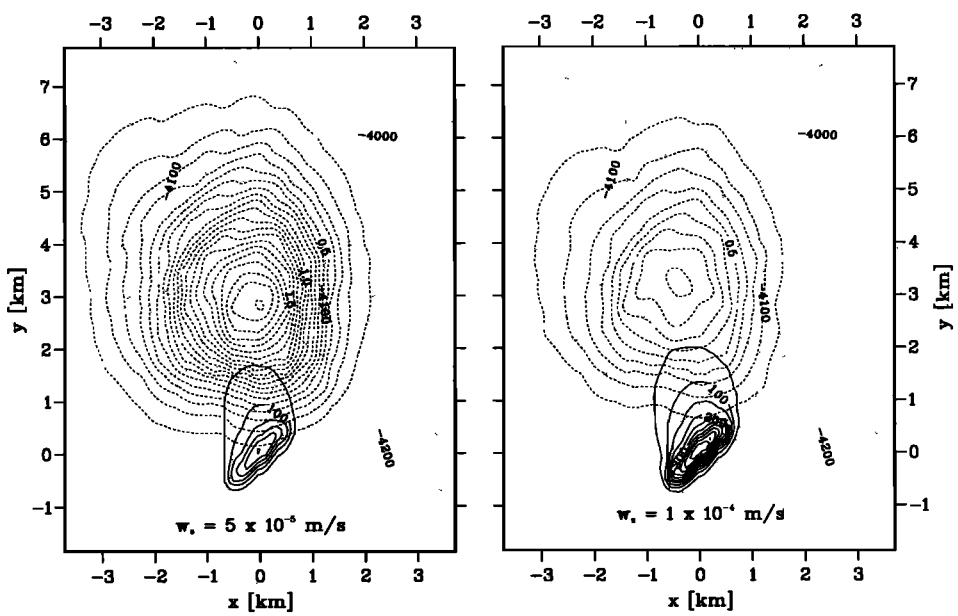

Figure 11. A horizontal section 1 m above bottom of sediment plumes (dashed lines) and the resedimentation patterns (solid lines) after 3 days. The units for concentration are milligrams per liter and for deposition, grams per square meter.

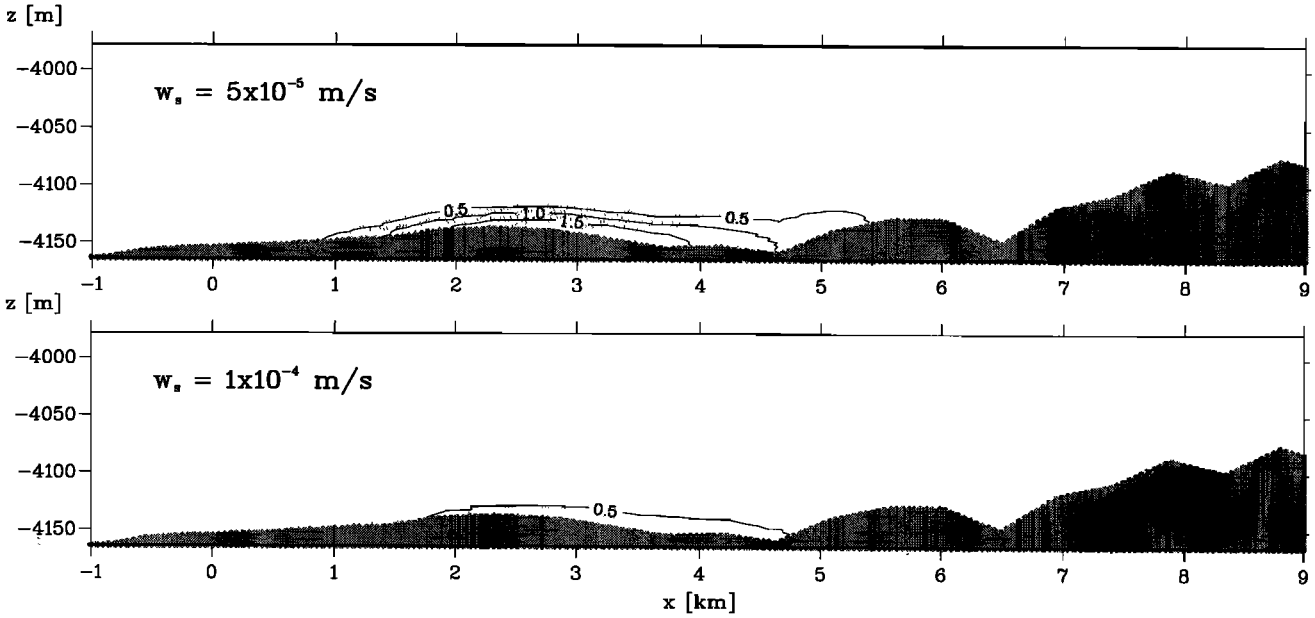

Figure 12. Vertical sections of sediment plumes in the north-south direction through the cordinate origin after 3 days. Concentrations are in milligrams per liter.

ures 11 and 12, respectively. The settling velocities are 10^{-4} m/s and 5×10^{-5} m/s (see Figure 9a).

Conclusions

The numerical transport model allows the simulation of sediment transport under the complicated unsteady conditions in the deep-sea bottom boundary layer over a varying topography. The model is independent of the specific features of the DISCOL area and, as such, can be applied to other typical deep-sea mining regions.

The use of available data from DEA allows the conclusion that the residence time of a sediment plume discharged at 10 kg/s by a single collector in a relatively small area (path length of about 1500 m) is of the order of 1.5–6 days for the settling velocity $w_s = 10^{-4}$ m/s.

Table 3. Maximum Concentrations $C_{\max}$ and Deposition $D_{\max}$ and the Associated Residence Time T_r for Different Mean Settling Velocities w_s

w_s, m/s	$C_{\max}$, mg/L	D_{max}, g/m^2	T_r, hours
	At 72 Hours		
5×10^{-4}	0.001	1563	6
1×10^{-4}	0.42	546	44
5×10^{-5}	2.02	306	118
1×10^{-5}	3.33	66	>144
	At 144 Hours		
5×10^{-4}	0.0	1563	6
1×10^{-4}	0.08	547	44
5×10^{-5}	0.24	307	118
1×10^{-5}	0.53	67	>144

Current Scenario 1, $\nu_{xc} = \nu_{yc} = 1.0$ m^2/s, $\delta = 10$ m.

This corresponds to emissions which take place during a small-scale impact experiment. The maximum sediment concentration in the plume at that time may be up to 50 times above ambient (taken as 10 μg/L). Even if the w_s is assumed to be a factor of 10 lower, the plume will dilute after 6 days to a similar concentration level (Table 3). The bed will be covered with > 100 g/m^2 of sediment in a radius of approximately 1–2 km from the collector tracks (Figure 11). Possible flocculation effects may accelerate the deposition because breakup effects are negligible. Data from mining tests or other specific experiments are scarce, and there are uncertainties in the model parameter values, such as the settling velocity, flocculation characteristics, and the discharge rate. Incomplete hydrodynamical measurements in the BBL lead to open questions, since a callibration cannot be performed.

Density flows and stratification effects in the direct vicinity of the source are not addressed directly in the described mesoscale model, but rather, through an assumption of the source distribution. It is necessary to quantify the portion of the suspended sediment which settles rapidly as a density flow near the source and the portion which remains in the water column for subsequent spreading by ambient currents [*Lavelle et al.*, 1981; *Baturin et al.*, 1991] in order to formulate the mesoscale model initial condition. A more precise initial condition requires measurements in the vicinity of the collector or an equivalent source. This would provide detailed information on the importance of density-induced flows and a more reliable description of the plume distribution at the time when passive dispersion begins. Future model developments, based on the results described by *Jankowski et al.*, [1994], will deal with this subject.

The flocculation and breakup processes in the discharged plume have not been measured in situ. Laboratory studies with sediments collected from the potential mining areas confirm the dependence of the effective settling velocity on the sediment concentration [*Ozturgut and Lavelle,* 1986]. Measurements are also needed to provide information on the particle properties, with special attention to the settling velocity distribution, densities, composition, and flocculation characteristics. Once data are available, an existing empirical settling velocity model, which has already given good results under complicated conditions in estuaries, will be applied. Further model developements will also include the simulation of the transport of other discharged substances which interact with the suspended sediments, for example, heavy metals released from the nodules.

A complete mesoscale plume dispersion verification is only possible during mining tests using prototype equipment [*Thiel,* 1991]. The model can be adapted to such emissions as far as they take place. Small-scale experiments planned in the second phase of the TUSCH project or already made during the international Benthic Impact Experiments by the National Oceanic and Atmospheric Administration could provide important information on the parameters controlling plume transport and its configuration in the vicinity of its source.

Acknowledgments. The research work was sponsored by the German Federal Ministry for Science and Technology (BMFT) within the interdisciplinary research group TUSCH under grant 03F0010B (Mesoskalige Stofftransporte im Pazifik als Folge des Tiefseebergbaus). The authors are solely responsible for the contents of this paper. The computer code TELEMAC3D was developed by the Electricité de France. The authors thank M. Markofsky for editing this paper.

References

Amann, H., The Red Sea Pilot Project: Lessons for future ocean mining, *Mar. Min.*, *8*, 1–22, 1989.

Armi, L., and R.C. Millard, Jr., The bottom boundary layer of the deep ocean, *J. Geophys. Res.*, *81*, 4983–4990, 1976.

Asper, V., Measuring the flux and sinking of marine snow aggregates, *Deep Sea Res., Part A*, *34*, 1–17, 1987.

Baturin, G.N., T.A. Demidova, Y.A. Kontar', and N.D. Kurlayev, The recovery and processing of the iron-manganese nodules and the turbidity of the bottom layer of the ocean, *Oceanology, Engl. Transl.*, *31*(4), 473–481, 1991.

Bischoff, J., and D. Piper, (Eds.), *Marine Geology and Oceanography of the Pacific Manganese Nodule Province*, 839 pp., Plenum, New York, 1979.

Bowden, K.F., Physical problems of the benthic boundary layer, *Geophys. Surv.*, *3*, 255–296, 1978.

Brockett, T., and C. Richards, Deep-sea mining simulator for environmental impact studies, *Sea Technol.*, *1994*(8), 77–82, 1994.

Csanady, G.T., On the 'resistance law' of a turbulent Ekman layer, *J. Atmos. Sci.*, *24*, 467–471, 1967.

Dyer, K.R., Sediment processes in estuaries: Future research requirements, *J. Geophys. Res.*, *94*, 14,327–14,332, 1989.

Friedlander, S.K., *Smoke, Dust and Haze*, 317 pp., John Wiley, New York, 1977.

Galland, J.-C., N. Goutal, and J.-M. Hervouet, TELEMAC: A new numerical model for solving shallow water equations, *Adv. Water Resour.*, *14*(3), 138–148, 1991.

Gill, A. E., *Atmosphere-Ocean Dynamics*, 662 pp., Academic, San Diego, Calif., 1982.

Halbach, P., G. Friedrich, and U. von Stackelberg, *The Manganese Nodule Belt of the Pacific Ocean*, 254 pp., Enke Verlag, Stuttgart, 1988.

Jankowski, J.A., A. Malcherek, and W. Zielke, Numerical modelling of sediment transport processes caused by deep sea mining discharges, in *Proceedings of the OCEANS 94 Conference, Brest*, vol. III, pp. 269–276, Inst. of Elec. and Electron. Eng., New York, 1994.

Jankowski, J.A., and W. Zielke, Mesoskalige Stofftransporte im Pazifik als Folge des Tiefseebergbaus, final report, 86 pp., Inst. für Strömungsmech. und ERiB, Univ. Hannover, Hannover, Germany, 1995.

Klein, H., Near-bottom currents in the deep Peru Basin, DISCOL Experimental Area, *Dt. Hydrogr. Z.*, *45*, 31–42, 1993.

Krone, R.B., Flume studies of the transport of sediment in estuarial shoaling processes, final report, Hydr. Eng. Lab., Univ. of Calif., Berkeley, 1962.

Krone, R.B., The significance of aggregate properties to transport processes, in *Estuarine Cohesive Sediment Dynamics, Coastal Estuarine Stud.*, vol. 14. edited by A.J. Mehta, pp. 66–84, 1986.

Kunzendorf, H. (Ed.), *Marine Mineral Exploration*, 300 pp., Elsevier, New York, 1986.

Kunzendorf, H., Proposed marine mineral exploration strategies for the nineties, *Mar. Min.*, *7*, 233–247, 1988.

Lavelle, J., Effects of boundary layer structure and macroparticle scavenging on the benthic deposition of fine sediment resuspended during nodule mining, final report, 39 pp., Natl. Oceanic and Atmos. Admin., Off. of Ocean and Coastal Resour. Manage., Pac. Mar. Environ. Lab., Seattle, Wash., 1987.

Lavelle, J., and E. Ozturgut, Dispersion of deep-sea mining particulates and their effect on light in ocean surface layers, *Mar. Min.*, *3*, 185–212, 1981.

Lavelle, J., E. Ozturgut, S. Swift, and B. Ericson, Dispersal and resedimentation of the benthic plume from deep-sea mining operations: A model with calibration, *Mar. Min.*, *3*, 59–93, 1981.

Lavelle, J., E. Ozturgut, E. Baker, and S. Swift, Discharge and surface plume measurements during manganese nodule mining tests in the North Equatorial Pacific, *Mar. Environ. Res.*, *7*, 51–70, 1982.

LeBlond, P., and L. Mysak, *Waves in the Ocean, Oceanogr. Ser.*, vol. 20, 602 pp., Elsevier, New York, 1978.

LeNormant, C., F. Lepeintre, C. Teisson, A. Malcherek, M. Markofsky, and W. Zielke, *Three dimensional modelling of estuarine processes*, in *MAST Days and Euromar Market, Proj. Rep.*, vol. 1, edited by K.-G. Barthel, M. Bohle-Carbonell, C. Fragakis and M. Weydert, European Union, Brussels, 1993.

Malcherek, A., Mathematische Modellierung von Strömungen und Stofftransportprozessen in Ästuaren, Ph.D. thesis, Univ. of Hannover, Hannover, Germany, 1995.

Malcherek, A., J.A. Jankowski, and H. Hoyme, SEACLOUD: Ein analytisches Modell zur Berechnung des mesoskaligen Stofftransports als Folge des Tiefseebergbaus, report, Inst. für Strömungsmech. und ERiB, Univ. Hannover, Hannover, Germany, 1992.

Malcherek, A., M. Markofsky, and W. Zielke, Numerical modelling of settling velocity variations in estuaries, *Arch. Hydrobiol.*, in press, 1996.

McCave, I., Size-spectra and aggregation of suspended particles in the deep ocean, *Deep Sea Res.*, *31*, 329–352, 1984.

McCave, I., and T.F. Gross, In-situ measurements of particle settling velocity, *Mar. Geol.*, *99*, 403–412, 1991.

Mofjeld, H., and W. Lavelle, Settling the length scale in a second-order closure model of the unstratified bottom boundary layer, *J. Phys. Oceanogr.*, *14*, 833–839, 1984.

Monin, A.S., and R.V. Ozmidov, *Turbulence in the Ocean*, 247 pp., D. Reidel, Norwell, Mass., 1985.

Nihoul, J.C.J., and S. Djenidi, Perspective in three-dimensional modelling of the marine system, in *Three-Dimensional Models of Marine and Estuarine Dynamics, Oceanogr. Ser.*, vol. 45, edited by J.C.J. Nihoul and B.M. Jamart, pp. 1–34, Elsevier, New York, 1987.

Ozturgut, E., and J.W. Lavelle, Settling analysis of fine sediments in salt water at concentrations low enough to preclude flocculation, *Mar. Geol.*, *69*, 353–362, 1986.

Ozturgut, E., J.W. Lavelle, and B. Erickson, Estimated discharge characteristics of a commercial nodule mining operation, *Mar. Min.*, *3*, 1–13, 1981.

Padan, J., Commercial recovery of deep seabed manganese nodules: Twenty years of accomplishments, *Mar. Min.*, *9*, 87–103, 1990.

Platzman, G., Ocean tides and related waves, in *Mathematical Problems in the Geophysical Sciences*, vol. 14, edited by W. Reid, pp. 239–291, Am. Math. Soc., Providence, R.I., 1971.

Pond, S., and G. Pickard, *Introductory Dynamical Oceanography*, 329 pp., Pergamon, Tarrytown, N.Y., 1983.

Sheng, Y., Mathematical modeling of three-dimensional coastal currents and sediment dispersion. Model development and application, *Tech. Rep. CERC-83-2*, 288 pp., U.S. Army Corps of Eng., Vicksburg, Miss., 1983.

Thiel, H., From MESEDA to DISCOL: A new approach to deep-sea mining risk assessments, *Mar. Min.*, *10*, 369–386, 1991.

Thiel, H., and G. Schriever, Cruise report DISCOL 1, SONNE-cruise 61, *Rep. 3*, 75 pp., Zentrum für Meeres- und Klimaforsch. der Univ. Hamburg, Hamburg, Germany, 1989.

Thiel, H., and G. Schriever, Deep-sea mining, environmental impact and the DISCOL project, *Ambio*, *19*, 245–250, 1990.

Thiel, H., E. Foell, and G. Schriever, Potential environmental effects of deep sea mining, *Rep. 26*, 243 pp., Zentrum für Meeres- und Klimaforsch. der Univ. Hamburg, Hamburg, Germany, 1991.

Thijsen, T., G. Glasby, A. Schmitz-Wiechowski, G. Friedrich, H. Kunzendorf, D. Müller, and H. Richter, Reconnaisance survey of manganese nodules from the northern sector of the Peru Basin, *Mar. Min.*, *2*, 385–428, 1981.

Trueblood, D., US Cruise report for BIE II, *Tech. Memo. NOS OCRM 4*, 51 pp., Natl. Ocean Serv., Natl. Oceanic and Atmos. Admin., Silver Spring, Md. 1993.

UNESCO, *International Oceanographic Tables*, vol. 4., *UNESCO Tech. Pap. Mar. Sci.*, *40*, 1987.

van Leussen, W., Aggregation of particles, settling velocities of mud flocs. A review, in *Physical Processes in Estuaries*, edited by J. Dronkers and W. van Leussen, pp. 347–403, Springer Verlag, New York, 1988.

van Leussen, W., Estuarine macroflocs and their role in fine-grained sediment transport, Ph.D. thesis, Univ. of Utrecht, Utrecht, Netherlands, 1994.

J.A. Jankowski, A. Malcherek and W. Zielke, Institut für Strömungsmechanik und ERiB, Universität Hannover, Appelstr. 9A, D-30167 Hannover, Germany, e-mail: jacek@appel012.hydromech.uni-hannover.de

(Received May 4, 1995; revised September 25, 1995; accepted November 11, 1995.)